Fish and Shellfish Immunology 90 (2019) 126–133

Contents lists available at ScienceDirect

Fish and Shellfish Immunology

journal homepage: www.elsevier.com/locate/fsi

Full length article

Molecular cloning of the Rab7 effector RILP (Rab-interacting lysosomal protein) in *Litopenaeus vannamei* and preliminary analysis of its role in white spot syndrome virus infection

Jixing Feng*, Denglai Li, Yongzheng Tang, Rongbin Du, Liming Liu

Laboratory of Pathology of Aquatic Animals, Yantai University, Yantai, 264005, PR China

ARTICLE INFO

Keywords:
Rab7 effector
RILP
White spot syndrome virus
Litopenaeus vannamei
RNA interfere

ABSTRACT

To investigate the role of the Rab7 effector RILP (Rab-interacting lysosomal protein) in white spot syndrome virus (WSSV) infection, the full-length cDNA of RILP (*Lv*RILP) was cloned in *Litopenaeus vannamei*, which consists of 1595 bp and encodes a polypeptide of 411 amino acids. Sequence analysis and multiple sequence alignment displayed that *Lv*RILP contained a conserved RILP region from 277 amino acid to 325 amino acid. Both the *Lv*RILP and Rab7 mRNA were most highly expressed in stomach and most lowly expressed in hemocyte, which were significantly up-regulated and exhibited similar kinetics post WSSV infection. The interaction of Rab7 with *Lv*RILP was verified by both GST Pull-down and ELISA. Meanwhile, the results of Pull-down assays showed that the GST-tagged VP28 (GST-VP28), His-tagged Rab7 (His-Rab7) and His-RILP formed a tripartite complex. After silencing by specific *Lv*RILP dsRNA, the *Lv*RILP mRNA level exhibited a significant reduction, and the expression levels of three WSSV genes *ie1*, *wsv477* and *vp28* all exhibited decreases at 24, 36 and 48 h post WSSV infection. These results suggested that the Rab7 effector RILP was involved in WSSV infection.

1. Introduction

It has been well documented that white spot syndrome virus (WSSV) applied endocytosis predominantly for entry into the host cell. This endocytosis pathway could be mediated by caveolin in hemocyte of both *Litopenaeus vannamei* and *Cherax quadricarinatus* [1,2]. However, in crayfish hematopoietic tissue, WSSV appears to enter by the clathrin-mediated endocytosis pathway that is responsible for viral uptake [3]. No matter what protein mediating the endocytosis pathway, the endosomes containing WSSV must be transported for the translocation to nuclei. Three different classes of molecular motors, including cytoplasmic dynein, kinesin and myosin might be adopted along the most convenient pathway for virus transport [4–6]. Among these three molecular motors, myosin interacts with actin filaments to move cargoes, while cytoplasmic dynein and kinesin use microtubule (MT) as track to move cargoes across the cytoplasm [7,8].

In the previous work, we have investigated the essential role of cytoplasmic dynein intermediate chain (DYNCI) in WSSV infection [9]. After knocking down DYNCI gene, the expression of WSSV genes was significantly delayed which indicated the essential role of cytoplasmic dynein in WSSV transport. In addition, the interaction between DYNCI and Rab7 was predicted in STRING database, however, this association could not be determined in co-immunoprecipitation using rabbit anti-DYNCI-PAbs and rabbit anti-Rab7 antibody respectively. This phenomenon showed the interaction between DYNCI and Rab7 to be indirect.

Accordingly, Rab7 is involved in governing multiple trafficking processes including the biogenesis of the lysosome, phagosome, autophagosome, and other lysosome-related organelle [10]. This role of Rab7 has been confirmed to be carried out by recruiting Rab7-interacting lysosomal protein (RILP), oxysterol-binding protein related protein 1L (ORP1L), cytoplasmic dynein and dynactin to form a complex to regulate MT minus-directed transport of endosomes [10,11]. Rab7 as a VP28 binding protein has also been identified to be involved in WSSV infection to *Penaeus monodon* and *L. vannamei* [12–15]. However, the information on the Rab7 effectors in shrimp and its role in WSSV transport was still limited.

In order to further investigate the role of Rab7 and its effectors in WSSV transport, rapid amplification of cDNA ends (RACE) was applied to clone the RILP cDNA sequence in *L. vannamei* (*Lv*RILP). The expression profile of Rab7 and *Lv*RILP in hemocyte was investigated during WSSV infection by quantitative real-time RT-PCR (qRT-PCR). The interaction between VP28, Rab7 and RILP was also examined. Finally, RNA interference (RNAi) was applied to knock down the

* Corresponding author.
E-mail address: jxfeng2014@ytu.edu.cn (J. Feng).

https://doi.org/10.1016/j.fsi.2019.04.306
Received 30 January 2019; Received in revised form 26 April 2019; Accepted 30 April 2019
Available online 03 May 2019

*Lv*RILP gene and its effect on WSSV infection was investigated. The resultant data would facilitate better understanding of WSSV transport in host cells.

2. Materials and methods

2.1. Shrimp

Adult shrimp (*L. vannamei*) with an average length of 15 cm were obtained from a commercial shrimp farm located in Yantai, Shandong, PR China and confirmed to be WSSV-free by two-step PCR with nested primer sets [16]. The shrimp were acclimated for 1 week in tanks filled with sea water of 30‰ salinity and provided with continuous aeration using electric air-pumping compressors. Half the tank water was changed at a time and the water was changed twice a week. The water temperature was 24 ± 1 °C.

2.2. Full-length cDNA cloning of LvRILP

The hemolymph was withdrawn with equal volume of modified Alsever solution (27 mM Na citrate, 336 mM NaCl, 115 mM glucose, 9 mM EDTA, pH 7.2) from the pericardial cavity of the randomly selected shrimp in each group. Hemocytes were collected by centrifuging at 400 × *g* for 10 min and washed twice by centrifugation using modified Alsever solution. The collected hemocytes were dissolved in 1 ml TRIzol® reagent (Life Technologies, USA) for total RNA isolation. The cDNA template used for RACE was synthesized from 2 μg total RNA according to the User Manual of SMART™ RACE cDNA Amplification Kit (Clontech, USA). Primers Deg-F and Deg-R were designed according to the conserved sequences from known RILP of twelve crustaceans, which were obtained from GenBank of NCBI under accession nos. EGI62411, XP_011166889, XP_011350254, XP_015516925, XP_313909, XP_015111190, XP_008196147, XP_011258524, XP_012266521, XP_013184185, XP_012243112 and XP_014272990 respectively, and used to amplify a partial cDNA. Based on the obtained partial cDNA sequence, the primer 3′-GSP and 5′-GSP were designed for 3′-RACE and 5′-RACE respectively. By ligation of the overlapping cDNA fragments, the full-length *Lv*RILP cDNA was obtained and confirmed by sequencing using the primers RILP-F and RILP-R. All the primers used in this part were listed in Table 1.

2.3. Sequence analysis

The cDNA sequence of *Lv*RILP and its deduced amino acid sequence were analyzed using the BLAST algorithm. The protein motif features were predicted by SMART (http://smart.embl-heidelberg.de/). An unrooted phylogenetic tree was constructed based on the sequences alignment by the neighbor-joining (NJ) algorithm using the Mega 4.0 program. The reliability of the branching was tested by using bootstrap re-sampling (1000 pseudo-replicates).

2.4. Distribution of LvRILP, Rab7 transcript and their expressions in response to WSSV infection

The hemocyte, muscle, hepatopancreas, heart, stomach, gill, intestine and lymphoid organ were individually sampled from healthy shrimp for RNA extraction. Each WSSV-free shrimp was injected with 1×10^6 virus copies diluted in 100 μl 0.01 M phosphate-buffered saline (PBS, pH 7.2) through the lateral area of the third abdominal segment. Hemocytes and stomach of shrimp at 6, 12, 18, 24, 36, 48, 60 and 72 h post infection (hpi) were collected respectively. The shrimp injected with WSSV were simultaneously selected for hemocytes and stomach sampling which were used as control and considered as sample at 0 hpi. RNA isolation and cDNA synthesis were performed as described in section 2.2. Finally, qRT-PCR was performed with the SYBR Green 2 × Master mix (TaKaRa, Japan) on a Roche LightCycler480 Real Time System (Roche, Switzerland) with RILP-qF, RILP-qR and Rab7-qF, Rab7-qR as primers. Elongation factor1-α gene obtained from GenBank of NCBI under accession no. GU136229 was applied as housekeeping gene and amplified using primers EF-1α-qF and EF-1α-qR. All the primers used in this part were listed in Table 1.

Table 1
Names and sequences of primers used in this paper.

Name	Sequence (5′–3′)
Deg-F	TGAAGGAGATCCTGCACGANMGNAAYGA
Deg-R	GGTCTCGGAGGACTTCTTCCANGGNGCRTC
3′-GSP	ACCAGTACAAGGTCCCATGCCCTATGAA
5′-GSP	CAGATAATGTGGCTCCGCTGTCGCTCTT
RILP-F	ATGCCGTACCAAATCGATTCGGAAC
RILP-R	TCAGGGGCGGCTAAGGTTAAGCAAG
RILP-His-F	TAGAATTCATGCCGTACCAAATCGATTC
RILP-His –R	CTGTCGACTCAGGGGCGGCTAAGGTTAAG
Rab 7-GST/His-F	CCGAATTCATGGCATCTCGCAAGAAGAT
Rab 7-GST/His-R	CTGTCGACTTAGCAAGAGCATGCATCCT
VP28-GST-F	CCGAATTCCGCACAGACAATATCGAGAC
VP28-GST-R	CTGTCGACTTACTCGGTCTCAGTGCCAG
RILP-qF	CACGTCCTCGTACATCCAGG
RILP-qR	GACTGTTCCCTCGGACTTGG
Rab7-qF	CGATTCATGGCGTGACGAGT
Rab7-qR	GCGAGCAATGGTCTGGAAAG
RILP-RNAi-T7-F	TAATACGACTCACTATAGGGCGAGGGAACAGTCATCCACT
RILP-RNAi-R	TCGAGATCAGACACACGAGC
RILP-RNAi-F	CGAGGGAACAGTCATCCACT
RILP-RNAi-T7-R	TAATACGACTCACTATAGGGTCGAGATCAGACACACGAGC
EF-1α-qF	TGCCCTGGACAACATCGAGC
EF-1α-qR	CGGGCACTGTTCCAATACCT
vp28-qF	GGGAACATTCAAGGTGTGGA
vp28-qR	GGTGAAGGAGGAGGTGTTGG
ie1-qF	AGCAAGTGGAGGTGCTATGT
ie1-qR	CCATGTCGATCAGTCTCTTC
wsv477-qF	GGCCAAGTCATGGAGATCTA
wsv477-qR	CCATCCACTTGGTTGCAGTA
Oligo dT	TTTTTTTTTTTTTTTTTTTTTTTTTVN

2.5. Expression of recombinant proteins

Primers RILP-His-F and RILP-His-R, Rab7-His/GST-F and Rab7-His/GST-R, VP28-GST-F and VP28-GST-R were used to amplify sequence of RILP, Rab7 and VP28. The amplified products were inserted into pET-28a/pGEX-4T-1 vector and expressed as His/GST-tagged fusion protein in *Escherichia coli* BL21 (DE3). Expression and purification of the recombinant proteins were performed according to the manual of HisTrap HP (GE Healthcare Life Sciences, USA) and BeyoGold™ GST-tag Purification Resin (Beyotime Biotech, China). The expression and purification of recombinant proteins was analyzed by 12% SDS-PAGE. The specificity of mouse anti-Rab7 monoclonal antibody (Mab) (raised against epitopes corresponding to amino acids 158 to 207 of Rab7 of human origin, Santa Cruz, USA) against Rab7 in hemocyte was identified by western blotting. All the primers used in this part were listed in Table 1.

2.6. Pull-down assays

To verify the interaction of Rab7 with *Lv*RILP, GST-tagged Rab7 (GST-Rab7) coupled beads were first incubated with 100 μM GTP for 10 min at room temperature and then washed twice by centrifuging at 1000 × *g* for 10 s. His-tagged RILP (His-RILP, 10 μg) diluted in 500 μl GST pull-down binding buffer (Tris-HCl, 50 mM; NaCl, 200 mM; EDTA, 1 mM; NP-40, 1%(v/v); DTT, 1 mM; $MgCl_2$, 10 mM, pH 8.0) was added to the beads and the incubation was carried out on a horizontal rotator at 4 °C overnight.

To investigate the cross-interaction between WSSV VP28, Rab7 and *Lv*RILP, His-Rab7 (10 μg), His-RILP (10 μg) as well as the mixture of His-Rab7 (10 μg) and His-RILP (10 μg), which were diluted in 500 μl

GST pull-down binding buffer, were incubated with GST-VP28 coupled beads respectively. GTP was added to the GST pull-down binding buffer with the final concentration of 100 μM. The incubation was carried out on a horizontal rotator at 4 °C overnight.

The GST-Rab7/VP28 beads were collected by centrifuging at 1000 × *g* for 10 s and washed twice by centrifugation using GST pull-down binding buffer. After extensive washing, the retained proteins with GST-Rab7 and GST-VP28 were analyzed by 12% SDS-PAGE. The retained His-Rab7 with GST-VP28 was analyzed by western blotting using mouse anti-Rab7 Mab.

2.7. ELISA

Flat-bottomed 96-well ELISA plates (Corning Costar, USA) were coated with 2 μg His-RILP (in 0.1 Mbicarbonate/carbonate buffer, pH 9.6; 100 μl per well) or 10 μg total hemocyte proteins which were extracted from hemocytes lysed by 20 mM HEPES pH 7.4, 150 mM NaCl, 5 mM $MgCl_2$, 1% NP-40 at 4 °C for 30 min. EDTA was added to the hemocyte lysate with a final concentration of 0.5 M to eliminate the endogenous enzyme background [17]. After incubating overnight at 4 °C, plates were washed thrice with PBST (PBS containing 0.05% Tween-20), and blocking buffer (PBST with additional 1% BSA) was added, followed by incubation for 2 h at 37 °C. After washing with PBST, various dilutions (0 ng, 100 ng, 200 ng, 400 ng, 800 ng) of His-Rab7 in blocking buffer were added to plates, followed by incubation for 1 h at 37 °C.

For testing the binding of His-Rab7 to His-RILP, plates were washed and a blocking buffer diluted mouse anti-Rab7 Mab was added (100 μl per well), followed by incubation for 1 h at 37 °C. To eliminate the background OD_{450} level caused by the binding of mouse anti-Rab7 Mab and Rab7 in hemocyte lysate, mouse anti-Rab7 Mab was replaced with mouse anti-6 × His Tag mouse Mab (Sangon Biotech, China) to test the binding of His-Rab7 to hemocyte lysate.

After washing, HRP-labeled goat anti-mouse antibody (Sigma-Aldrich, USA) was added to plates, and reaction mixtures incubated for an additional 1 h at 37 °C. The reaction was visualized using the HRP substrate TMB (3,3′,5,5′-tetramethylbenzidine; Sangon Biotech). An ELISA reader (Biotech, USA) was used to read the absorbance immediately at 450 nm. Each experiment was done in triplicate. The data were given in terms of OD_{450} as means ± standard deviation (SD) (n = 3) and subjected to oone-way ANOVA followed by a multiple comparison. The *p* values less than 0.05 were considered statistically significant.

2.8. Double-stranded (ds) RNA-mediated RNAi

E-RNAi web-service (https://www.dkfz.de/signaling/e-rnai3/) was applied to identify the optimized RNAi target-sites of *Lv*RILP dsRNA that was from 411 bp to 896 bp in the open reading frame (ORF). *Lv*RILP dsRNA was prepared using T7 RiboMAX (Promega, USA) according to the protocols described in previous study [18]. The synthesized dsRNA was qualified by agarose gel electrophoresis and quantified by a nucleotide quantification machine, Nanodrop 2000™ (Thermo Scientific, USA). GFP dsRNA was synthesized as control. The primers used to synthesize *Lv*RILP dsRNA and GFP dsRNA are listed in Table 1.

Shrimp were injected with *Lv*RILP dsRNA at a concentration of 1 μg/g shrimp, while shrimp injected with GFP dsRNA were used as control. A second injection was administered at 24 h after the first one. At 12, 24, 36, 48, 60 and 72 h post the first challenge (hpc) with dsRNA, 6 shrimp were randomly selected from both the *Lv*RILP and GFP dsRNA injected groups for hemocytes collection. The silencing effects on *Lv*RILP in hemocytes at each time point were examined at mRNA levels by qRT-PCR. The elongation factor1-α gene was used as internal control in qRT-PCR.

2.9. Quantification of viral genes expression

Based on the silencing effect on *Lv*RILP after injections of dsRNA, the experimental shrimp were injected with 1×10^6 WSSV copies diluted in 100 μl PBS at 12 h post the second injection of dsRNA and the shrimp administered with GFP dsRNA were also performed virus challenge as control. The hemocytes were collected for total RNA extraction at 12, 24, 36 and 48 hpi. In order to investigate the effect of *Lv*RILP silencing on the transcription of viral genes, the expression levels of *ie1*, *wsv477* and *vp28* were examined as described in section 2.7.

2.10. Statistical analysis

All the gene expression levels were determined in three replicates of qRT-PCR experiment. The comparative Ct method ($2^{-\triangle\triangle Ct}$ method) was used to analyze the relative expression level. The data were given in terms of relative mRNA expression level as means ± SD (n = 3) and subjected to one-way analysis of variance (one-way ANOVA) followed by a multiple comparison. The *p* values less than 0.05 were considered statistically significant.

3. Results

3.1. Characters of LvRILP cDNA and its deduced amino acids

A full-length *Lv*RILP cDNA was obtained by the procedures of RT-PCR and RACE. The cDNA was 1595 bp in length, containing a 1236 bp ORF which encoded 411 amino acids. The cDNA contained a 97 bp 5′-untranslated region and a 262 bp 3′-untranslated region. The predicted protein molecular mass was 47.12 kDa with an estimated isoelectric point of 4.85.

SMART prediction revealed that *Lv*RILP contained a conserved domain namely Jnk-SapK_ap_N from 23 amino acid to 168 amino acid, a RILP region from 277 amino acid to 325 amino acid, and three low complexity regions (Figs. 1 and 2).

Blast homology analysis showed that the deduced amino acid sequence of *Lv*RILP shared high identities with invertebrate RILP, including *Daphnia pulex* RILP (44%), *Drosophila navojoa* RILP isoform X1 (43%), *Acromyrmex echinatior* RILP (51%), *Solenopsis invicta* isoform X1 (51%), *Ooceraea biroi* isoform X1 (50%). Multiple alignments of *Lv*RILP with several invertebrate RILP showed that *Lv*RILP displayed several

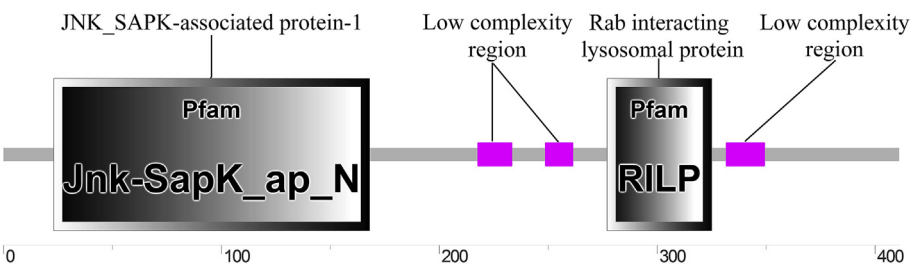

Fig. 1. Conserved domains and motifs predicted by SMART in the deduced amino acid sequence of *Lv*RILP. The line across the bottom represents the location of amino acid residues.

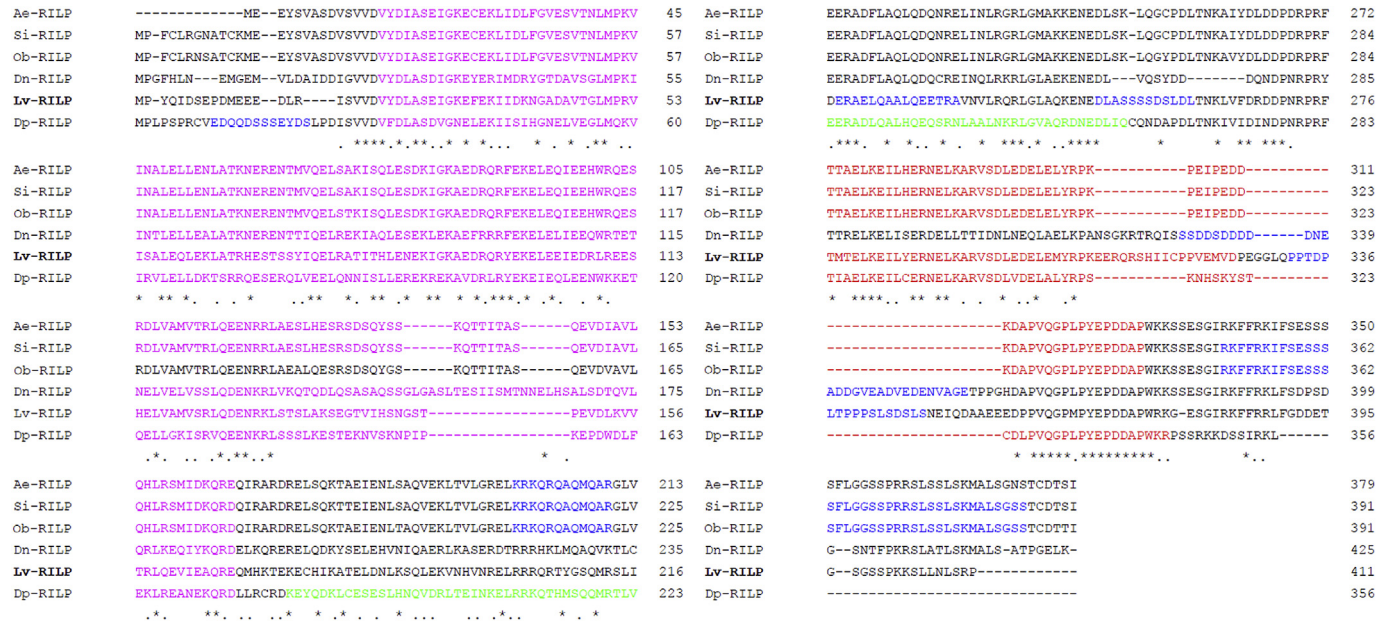

Fig. 2. Multiple sequence alignment of the predicted amino acid sequences of *Lv*RILP with that of several other invertebrate organisms. The conserved signature motifs Jnk-SapK_ap_N domain, RILP region and coiled coil region and low complexity regions are shown in pink, red, green and blue characters respectively. Amino acid conservation across alignments is shown as (*), () and (.) for identical, conserved and semi-conserved respectively. The abbreviations represent the species scientific names: Ae-*Acromyrmex echinatior* (EGI62411), Si-*Solenopsis invicta* (XP_011166889), Ob-*Ooceraea biroi* (XP_011350253), Dn-*Drosophila navojoa* (XP_017965091), Lv- *Litopenaeus vannamei*, Dp-*Daphnia pulex* (EFX68439). (For interpretation of the references to colour in this figure legend, the reader is referred to the Web version of this article.)

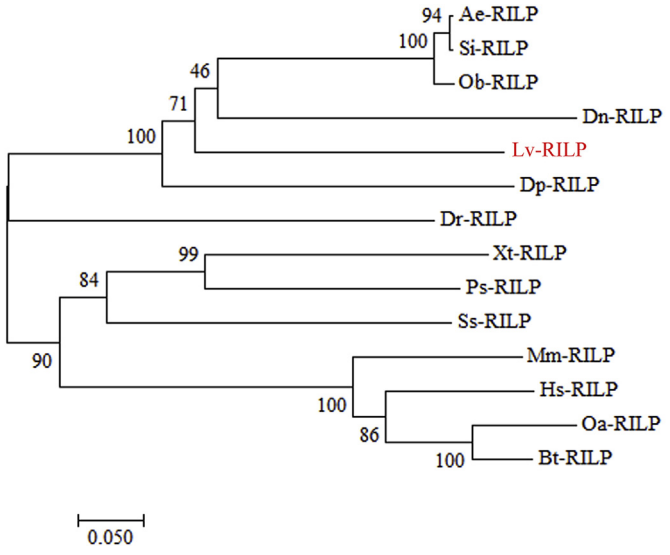

Fig. 3. Neighbour-joining phylogenetic tree of RILP amino acid sequences from different species. The cloned *Lv*RILP was indicated in red characters. The RILP are from *Homo sapiens* (AAH04961), *Mus musculus* (NP_001025109), *Ovis aries* (XP_014953794), *Salmo salar* (NP_001133493), *Bos taurus* (XP_002695729), *Danio rerio* (NP_001073132), *Xenopus tropicalis* (NP_001106596), *Pelodiscus sinensis* (XP_006127094), *Acromyrmex echinatior* (EGI62411), *Solenopsis invicta* (XP_011166889), *Ooceraea biroi* (XP_011350253), *Drosophila navojoa* (XP_017965091), *Daphnia pulex* (EFX68439), *L. vannamei*. (For interpretation of the references to colour in this figure legend, the reader is referred to the Web version of this article.)

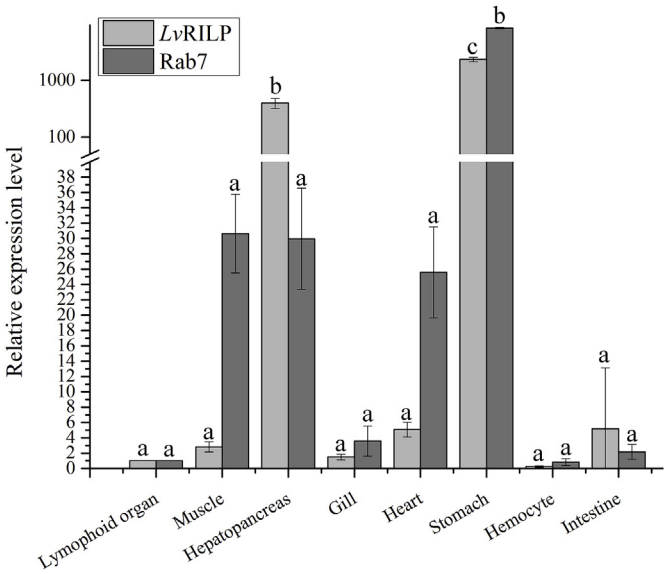

Fig. 4. Distribution of *Lv*RILP and Rab7 transcript in healthy *L. vannamei*. Each symbol and vertical bars represented the mean ± SD (n = 3). The different letters above the column indicate significant differences ($p < 0.05$) among the gene expression levels in different tissues.

highly conserved features possessed by RILP, including Jnk-SapK_ap_N domain, RILP region and several low complexity regions (Fig. 1). Fourteen sequences of available animal RILP proteins were used for the phylogenetic tree construction with NJ method. All the members of RILP were mainly clustered into two groups. *Lv*RILP was in the same subgroup with five other arthropod RILP homologues and the RILP of zebra fish (*Danio rerio*). The rest vertebrate RILP were in the same group (Fig. 3).

3.2. Expression profile of LvRILP and Rab7 in healthy shrimp and against WSSV infection in hemocyte

The *Lv*RILP and Rab7 gene transcript were expressed in all test samples. The highest mRNA expression level of both *Lv*RILP and Rab7 were detected in stomach. Much lower expression levels were found in hepatopancreas, muscle, heart, gill, lymphoid organ and intestine.

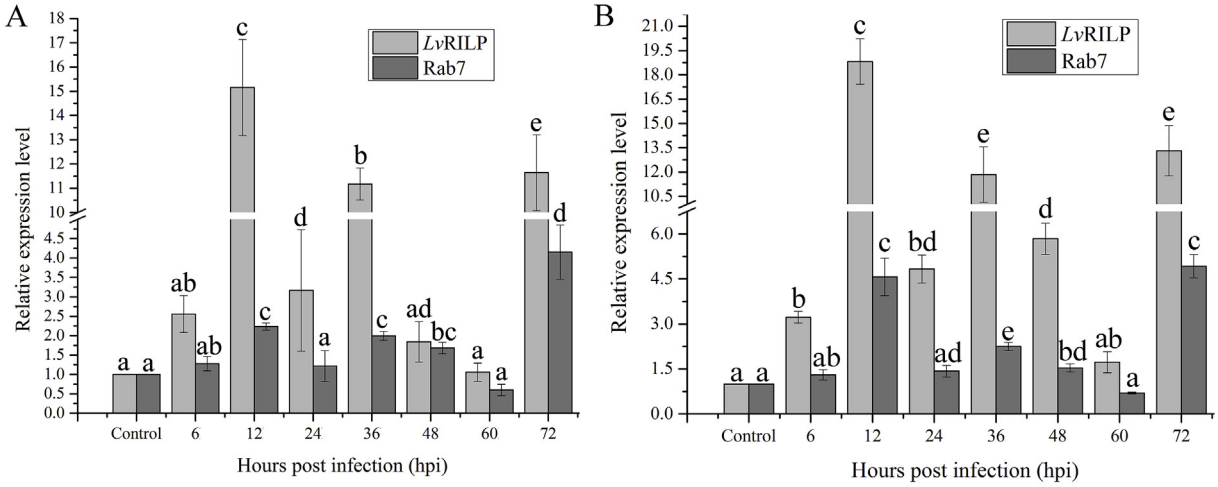

Fig. 5. Quantification of relative mRNA expression of *Lv*RILP and Rab7 in hemocytes (A) and stomach (B) after WSSV infection by qRT-PCR. Each symbol and vertical bars represented the mean ± SD (n = 3) and a, b, c, d and e indicate significant differences ($p < 0.05$) among the expression levels *Lv*RILP and Rab7 gene at different time points.

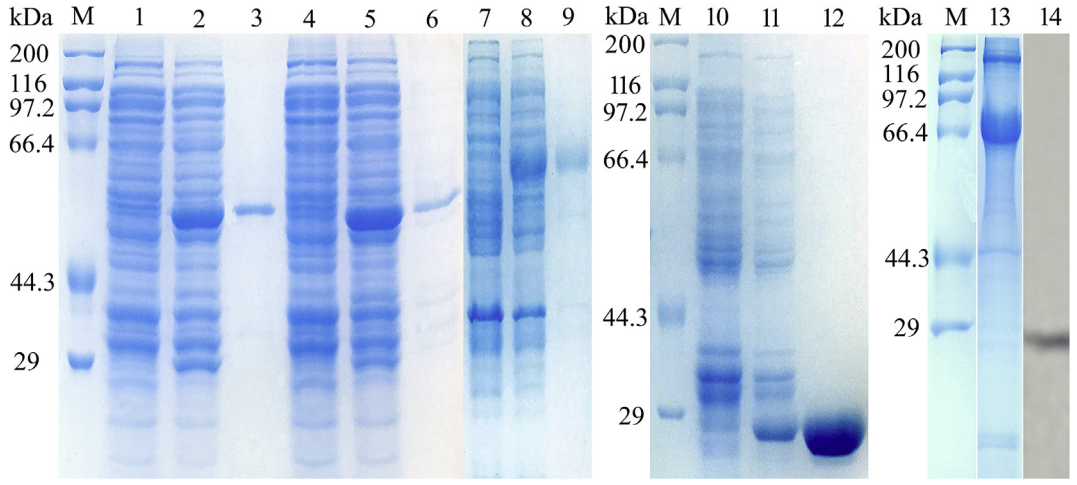

Fig. 6. SDS-PAGE and western blotting confirm the expression of recombinant proteins and the specificity of mouse anti-Rab7 Mab. Lane M, Molecular mass marker; lane 1, 4, 7, 10, protein profile of uninduced BL21 cell lysate; lane 2, 5, 8, 11, protein profile of induced BL21 cell lysate; lane 3, 6, 9, 12, purified GST-Rab7, GST-VP28, His-RILP and His-Rab7; lane 13, protein profile of hemocyte lysate; lane 14, mouse anti-Rab7 Mab recognized Rab7 in hemocytes.

Hemocyte exhibited the lowest mRNA expression level of both *Lv*RILP and Rab7 (Fig. 4).

Post WSSV infection, both the *Lv*RILP and Rab7 mRNA in hemocyte and stomach were significantly up-regulated. In hemocyte, the expression levels of *Lv*RILP gene were all significantly higher compared to that in control shrimp at 12, 36 and 72 hpi, while, the expression levels of Rab7 gene were significantly up-regulated at 12, 36, 48 and 72 hpi (Fig. 5A). In stomach, the expression levels of *Lv*RILP gene were all significantly higher compared to that in control shrimp at 6, 12, 36, 48 and 72 hpi and the expression levels of Rab7 gene were significantly up-regulated at 12, 36 and 72 hpi (Fig. 5B). The overall expression profile of *Lv*RILP gene exhibited a similar kinetics to the Rab7 gene in hemocyte and stomach post WSSV infection. However, the expression level range of the *Lv*RILP gene was larger than that of the Rab7 gene.

3.3. Expression of recombinant proteins and characterization of the specificity of mouse anti-Rab7 Mab

GST-Rab7, GST-VP28, His-RILP and His-Rab7 were successfully expressed in *E. coli* BL21 (DE3) respectively with expected molecular weights (Fig. 6, lane 2, 5, 8, 11). High purity His-RILP and His-Rab7 were obtained by nickel chelate affinity chromatography (Fig. 6, lane 9, 12), while, high purity GST-Rab7 and GST-VP28 were obtained by glutathione affinity chromatography (Fig. 6, lane 3, 6). The mouse anti-Rab7 Mab was identified to recognize Rab7 in hemocyte by western blotting (Fig. 6, lane 14).

3.4. Confirmation of the Rab7 binding to RILP by GST pull-down assay and ELISA

SDS-PAGE revealed that GST-Rab7 could efficiently pull down His-RILP in the presence of GTP, indicating the interacting of Rab7 with RILP was in a GTP-dependent manner (Fig. 8, lane 2).

Increasing His-Rab7 concentration in ELISAs enhanced its ability to bind to His-RILP and the hemocyte lysate, whereas for control protein, OD value was approximately constant when His-Rab7 concentrations increased. Therefore, His-Rab7 binding to both His-RILP and hemocyte lysate was specific and dose-dependent (Fig. 7).

3.5. The VP28-Rab7-RILP tripartite complex

To study whether the interaction between VP28 and Rab7 as well as RILP is direct, we used purified GST-VP28 to pull down purified His-Rab7 and His-RILP respectively. These experiments revealed that, GST-

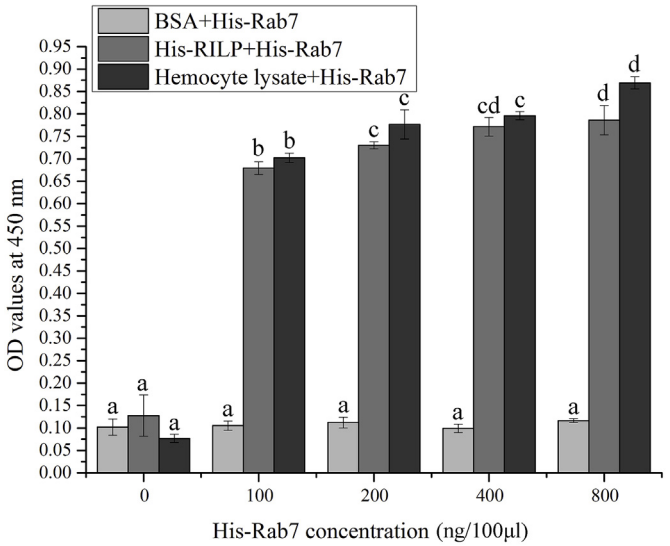

Fig. 7. ELISA assays demonstrated that Rab7 binding to RILP was specific. His-RILP (2 μg/well), BSA (2 μg/well) and hemocyte lysate (10 μg/well) were coated to a 96-well plate and incubated with various amounts of purified His-Rab7 (0 ng, 100 ng, 200 ng, 400 ng, 800 ng). Each column and vertical bar represents the mean ± SD of triplicate determinations. The different letters above the column indicate significant differences ($p < 0.05$) among the OD_{450} values at different His-Rab7 concentrations for each coated protein.

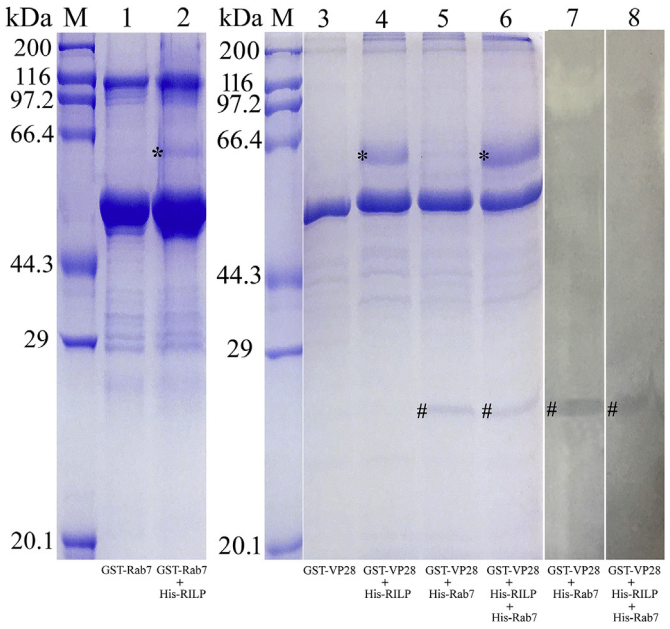

Fig. 8. SDS-PAGE and western blotting cinfirmed the cross-interaction between RILP, VP28 and Rab7. All the lanes in western blotting were incubated with mouse anti-Rab7 Mab. The positive bands indicating His-Rab7 and His-RILP are shown as (#) and (*) respectively. Lane M, Molecular mass marker; lane 1, protein profile of glutathione beads coupled with purified GST-Rab7; lane 2, the profile of retained proteins with purified GST-Rab7 and His-RILP; lane 3, protein profile of glutathione beads coupled with purified GST-VP28; lane 4, 5, 6, the profile of retained proteins with purified GST-VP28 and His-RILP, His-Rab7 as well as the mixture of His-RILP and His-Rab7 respectively; lane 7, 8, mouse anti-Rab7 Mab recognized His-Rab7 of lane 5, 6 in SDS-PAGE.

VP28 efficiently pulled down His-Rab7 (Fig. 8, lane 5, 7) and His-RILP (Fig. 8, lane 4) respectively. Furthermore, GST-VP28 pulled down both His-Rab7 and His-RILP indicating that GST-VP28, His-Rab7 and His-RILP formed a tripartite complex through pairwise interaction between these three proteins (Fig. 8, lane 6, 8).

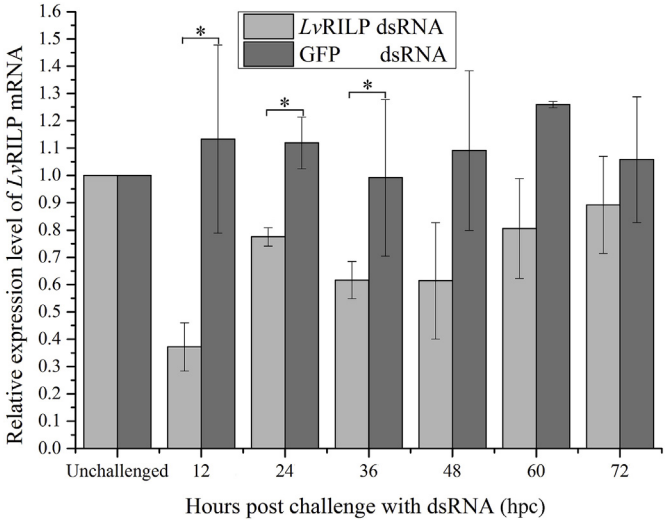

Fig. 9. Effects of dsRNA-mediated *Lv*RILP silencing in shrimp hemocytes detected by qRT-PCR. The asterisk represents the statistical significance ($p < 0.05$) compared to the control. Each symbol and vertical bars represented the mean ± SD (n = 3).

3.6. Silence of LvRILP gene by dsRNA-mediated RNAi in hemocytes

At 12 hpc, *Lv*RILP mRNA level in hemocytes was silenced by 1/3, however, which bounced back to about 7/10 at 24 hpc compared to the control group. While a second injection with *Lv*RILP dsRNA was administered, its mRNA expression was silenced and maintained at a lower level with approximate 3/5 of the control level at 36 hpc (Fig. 9). For shrimps that received GFP dsRNA, the *Lv*RILP mRNA expression in hemocytes did not show significant change at any detection time.

3.7. Delay of WSSV genes expression after the LvRILP gene silence

Post WSSV infection, the expression level of the virus immediate early gene (*ie1*), early gene (*wsv477*), and late gene (*vp28*) were all significantly decreased in the *Lv*RILP gene knockdown hemocytes. At 24, 36 and 48 hpi, the expression levels of *ie1*, *wsv477* and *vp28* in hemocytes of WSSV-infected shrimp exhibited the decreases with approximate 1/3000, 1/50, 1/25; 1/214, 1/20, 1/20; 1/11, 1/7, 1/4 of the control level respectively (Fig. 10).

4. Discussion

In the present work, an *Lv*RILP cDNA was cloned from the hemocyte of *L. vannamei* by RACE technique. This is the first evidence that RILP, which has been verified in regulation of the endicytic traffic, participates in WSSV infection [19,20]. SMART prediction revealed that *Lv*RILP contains a conserved domain namely Rab interacting lysosomal protein at its C-terminus comprising one coiled-coil region (278 amino acid to 306 amino acid) that specifically binds Rab7 (GTP bound form) [11]. Meanwhile, it has been well documented that one coiled-coil region (58 amino acid to 251 amino acid) locates at RILP N-terminus which interacts with the most C-terminal region of $p150^{Glued}$ (a subunit of dynactin) to recruit the cytoplasmic dynein motor complex to endosomes [11,21]. These suggested that *Lv*RILP was a typical member of Rab interacting lysosomal protein family.

The previous investigations about the relationship between protein-protein interactions suggested that genes with similar expression profiles were more likely to encode interacting proteins [22,23]. In the present study, the mRNA expression of Rab7 and *Lv*RILP displayed similar distribution in tissues and up-regulated profiles post WSSV challenge. Meanwhile, the results of GST Pull-down and ELISA

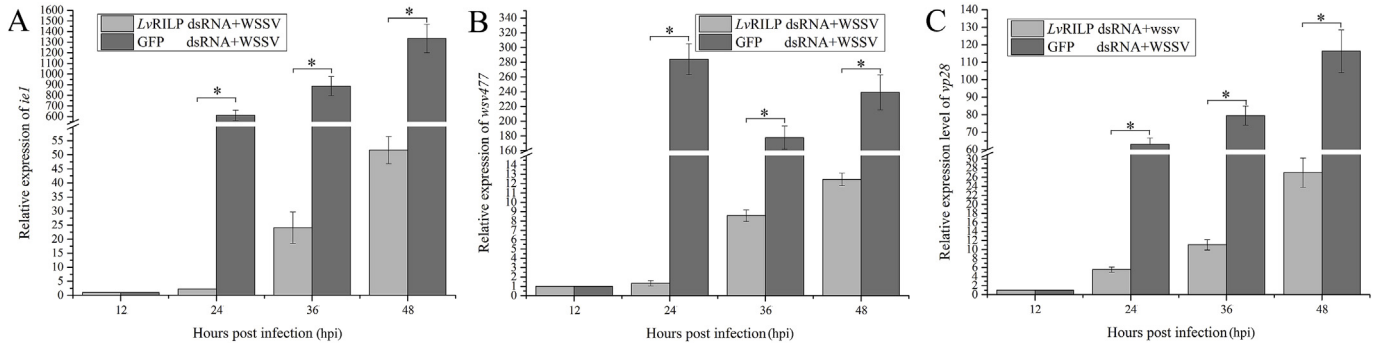

Fig. 10. Effects of dsRNA-mediated *Lv*RILP silence on *ie1* (A), *wsv477* (B) and *vp28* (C) expression in hemocytes detected by qRT-PCR. *Lv*RILP or GFP dsRNA were double-injected, along with purified WSSV at 12 h post the second injection of dsRNA. The asterisk represents the statistical significance ($p < 0.05$) compared to the control. Each symbol and vertical bars represented the mean ± SD (n = 3).

confirmed the specific interaction between Rab7 and RILP which suggested that a primate and canonical endosome traffic pathway existed in shrimp *L. vannamei*.

WSSV has been identified to adopt the caveolae-mediated endocytosis to enter shrimp hemocyte, and the virions could be localized in early endosome [1]. In the previous work, we have investigated the essential role of DYNCI in WSSV infection [9]. Meanwhile, the Rab7 effector protein RILP controls lysosomal transport by inducing the recruitment of dynein-dynactin motors [24–26]. These results may open the way for the investigation of complex events in the transport of WSSV across host cells. However, the activation of endosomal dynein motors is accomplished by stepwise assembly of Rab7-RILP-p150^{Glued} in mammalian cells [10,21,27]. In shrimp, the information about dynactin and its subunit p150^{Glued} was still limited. To decipher the transport of WSSV in host cells, much more works on the relationship between WSSV and cytoplasmic dynein motor need to be done in future. Recently, the decoding of the *L. vannamei* genome will provide an insight into the investigation of WSSV infection processes involved by dynactin [28].

It has been well documented that Rab7 mediates attachment of late endosomes to cytoplasmic dynein motor through the recruitment of RILP. Next, the Rab7-RILP complex is transferred by ORP1L to βIII spectrin for starting the translocation to microtubules through the interaction between βIII spectrin and dynein [21,29,30]. In this paper, dsRNA-mediated RNAi which was used to knock down *Lv*RILP gene further confirmed the involving of RILP in WSSV infection. Combined with the essential role of cytoplasmic dynein in WSSV infection investigated in our previous research, the significant decreasing of WSSV replication might be due to the hindrance of WSSV transport in *Lv*RILP-silenced hemocytes.

A model for the WSSV life cycle and morphogenesis has been documented that WSSV escapes from the late endosome to reach endoplasmic reticulum (ER) and further enter host nuclei for replication to avoid the fate to the degradation pathway [31,32]. Throughout this process,ORP1L conformation, which is sensed by the under low cholesterol conditions in ER, induces the formation of endoplasmic ER-late endosome membrane contact sites at which the vesicle-associated membrane protein-associated ER protein can interact with the Rab7-RILP complex to remove p150^{Glued} and associated motors [33–35]. To decipher WSSV trafficking in host cells, the investigations of proteins such as the Rab7 effectors RILP and ORP1L involved in intracellular endosome distributions need to be done in future.

Acknowledgements

This work was supported by Shandong Provincial Natural Science Foundation, China (ZR2015CL048), Shandong Province Agricultural Innovation Team (SDAIT-12-03) and Hainan Provincial Hey Research and Development Program (ZDYF2018028).

References

[1] Z.J. Huang, S.T. Kang, J.H. Leu, L.L. Chen, Endocytic pathway is indicated for white spot syndrome virus (WSSV) entry in shrimp, Fish Shellfish Immunol. 35 (2013) 707–715.
[2] H. Duan, S. Jin, Y. Zhang, F. Li, J. Xiang, Granulocytes of the red claw crayfish *Cherax quadricarinatus* can endocytose beads, *E. coli* and wssv, but in different ways, Dev. Comp. Immunol. 46 (2014) 186–193.
[3] J. Huang, F. Li, J. Wu, F. Yang, White spot syndrome virus enters crayfish hematopoietic tissue cells via Clathrin-mediated endocytosis, Virology 486 (2015) 35–43.
[4] J.G. Gindhart, Towards an understanding of kinesin-1 dependent transport pathways through the study of protein-protein interactions, Briefings Funct. Genomics Proteomics 5 (2006) 74–86.
[5] P.A. Harries, J.W. Park, N. Sasaki, K.D. Ballard, A.J. Maule, R.S. Nelson, Differing requirements for actin and myosin by plant viruses for sustained intercellular movement, Proc. Natl. Acad. Sci. U.S.A. 106 (2009) 17594–17599.
[6] M. Schliwa, G. Woehlke, Molecular motors, Nature 422 (2003) 759–765.
[7] D.D. Hackney, The kinetic cycles of myosin, kinesin, and dynein, Annu. Rev. Physiol. 58 (1996) 731–750.
[8] W. Lu, V.I. Gelfand, Moonlighting motors: kinesin, dynein, and cell polarity, Trends Cell Biol. 27 (2017) 505–514.
[9] J. Feng, X. Tang, W. Zhan, Cloning and characterization of cytoplasmic dynein intermediate chain in *Fenneropenaeus chinensis* and its essential role in white spot syndrome virus infection, Fish Shellfish Immunol. 39 (2014) 407–414.
[10] T. Wang, Z. Ming, W. Xiaochun, W. Hong, Rab7: role of its protein interaction cascades in endo-lysosomal traffic, Cell. Signal. 23 (2011) 516–521.
[11] G. Cantalupo, P. Alifano, V. Roberti, C.B. Bruni, C. Bucci, Rab-interacting lysosomal protein (RILP): the Rab7 effector required for transport to lysosomes, EMBO J. 20 (2001) 683–693.
[12] K. Sritunyalucksana, W. Wannapapho, C.F. Lo, T.W. Flegel, PmRab7 is a VP28-binding protein involved in white spot syndrome virus infection in shrimp, J. Virol. 80 (2006) 10734–10742.
[13] Á.R. Píndaro, M.R.C. Humberto, M.B.F. Javier, E.B.C. Marcial, Silencing pacific white shrimp *Litopenaeus vannamei Lv*Rab7 reduces mortality in brooders challenged with white spot syndrome virus, Aquacult. Res. 44 (2013) 772–782.
[14] P. Attasart, R. Kaewkhaw, C. Chimwai, U. Kongphom, O. Namramoon, S. Panyim, Inhibition of white spot syndrome virus replication in *Penaeus monodon* by combined silencing of viral rr2 and shrimp PmRab7, Virus Res. 145 (2009) 127–133.
[15] C. Ongvarrasopone, M. Chanasakulniyom, K. Sritunyalucksana, S. Panyim, Suppression of PmRab7 by dsRNA inhibits WSSV or YHV infection in shrimp, Mar. Biotechnol. 10 (2008) 374–381.
[16] C.F. Lo, J.H. Leu, C.H. Ho, C.H. Chen, S.E. Peng, Y.T. Chen, C.M. Chou, P.Y. Yeh, C.J. Huang, H.Y. Chou, C.H. Wang, G.H. Kou, Detection of baculovirus associated with white spot syndrome (WSBV) in penaeid shrimps using polymerase chain reaction, Dis. Aquat. Org. 25 (1996) 133–141.
[17] W. Zhan, X. Wang, J. Chen, J. Xing, H. Fukuda, Elimination of shrimp endogenous alkaline phosphatase background and development of enzyme immunoassays for the detection of white spot syndrome virus (WSSV), Aquaculture 239 (2004) 15–21.
[18] W. Yingvilasprasert, P. Supungul, A. Tassanakajon, *Pm*TBC1D20, a Rab GTPase-activating protein from the black tiger shrimp, *Penaeus monodon*, is involved in white spot syndrome virus infection, Dev. Comp. Immunol. 42 (2014) 302–310.
[19] J. Neefjes, M.M.L. Jongsma, I. Berlin, Stop or go? Endosome positioning in the establishment of compartment architecture, dynamics, and function, Trends Cell Biol. 27 (2017) 580–594.
[20] J.S. Bonifacino, J. Neefjes, Moving and positioning the endolysosomal system, Curr. Opin. Cell Biol. 47 (2017) 1–8.
[21] M. Johansson, N. Rocha, W. Zwart, I. Jordens, L. Janssen, C. Kuij, V.M. Olkkonen, J. Neefjes, Activation of endosomal dynein motors by stepwise assembly of Rab7-RILP-p150^{Glued}, ORP1L, and the receptor betalll spectrin, J. Cell Biol. 176 (2007) 459–471.
[22] H. Ge, Z. Liu, G.M. Church, M. Vidal, Correlation between transcriptome and interactome mapping data from *Saccharomyces cerevisiae*, Nat. Genet. 29 (2001) 482–486.

[23] M. Wang, J. Yang, Z. Zhou, L. Qiu, L. Wang, H. Zhang, Y. Gao, X. Wang, L. Zhang, J. Zhao, L. Song, A primitive Toll-like receptor signaling pathway in mollusk Zhikong scallop *Chlamys farreri*, Dev. Comp. Immunol. 35 (2011) 511–520.
[24] I. Jordens, M. Fernandez-Borja, M. Marsman, S. Dusseljee, L. Janssen, J. Calafat, H. Janssen, R. Wubbolts, J. Neefjes, The Rab7 effector protein RILP controls lysosomal transport by inducing the recruitment of dynein-dynactin motors, Curr. Biol. 11 (2001) 1680–1685.
[25] S.L. Reck-Peterson, W.B. Redwine, R.D. Vale, A.P. Carter, The cytoplasmic dynein transport machinery and its many cargoes, Nat. Rev. Mol. Cell Biol. 19 (2018) 382–398.
[26] X. Ma, K. Liu, J. Li, H. Li, J. Li, Y. Liu, C. Yang, H. Liang, A non-canonical GTPase interaction enables ORP1L-Rab7-RILP complex formation and late endosome positioning, J. Biol. Chem. 293 (2018) 14155–14164.
[27] F. Guerra, C. Bucci, Multiple roles of the small GTPase Rab7, Cells 5 (2016) 34.
[28] X. Zhang, J. Yuan, Y. Sun, S. Li, Y. Gao, Y. Yu, C. Liu, Q. Wang, X. Lv, X. Zhang, K.Y. Ma, X. Wang, W. Lin, L. Wang, X. Zhu, C. Zhang, J. Zhang, S. Jin, K. Yu, J. Kong, P. Xu, J. Chen, H. Zhang, P. Sorgeloos, A. Sagi, A. Alcivar-Warren, Z. Liu, L. Wang, J. Ruan, K.H. Chu, B. Liu, F. Li, J. Xiang, Penaeid shrimp genome provides insights into benthic adaptation and frequent molting, Nat. Commun. 10 (2019) 356.
[29] S. Pankiv, E.A. Alemu, A. Brech, J.A. Bruun, T. Lamark, A. Overvatn, G. Bjørkøy, T. Johansen, FYCO1 is a Rab7 effector that binds to LC3 and PI3P to mediate microtubule plus end-directed vesicle transport, J. Cell Biol. 188 (2010) 253–269.
[30] E.B. Dewey, C.A. Johnston, Diverse mitotic functions of the cytoskeletal cross-linking protein Shortstop suggest a role in Dynein/Dynactin activity, Mol. Biol. Cell 28 (2017) 2555–2568.
[31] C.M. Escobedo-Bonilla, V. Alday-Sanz, M. Wille, P. Sorgeloos, M.B. Pensaert, H.J. Nauwynck, A review on the morphology, molecular characterization, morphogenesis and pathogenesis of white spot syndrome virus, J. Fish Dis. 31 (2008) 1–18.
[32] B. Verbruggen, L. Bickley, R. van Aerle, K. Bateman, G. Stentiford, E. Santos, C. Tyler, Molecular mechanisms of white spot syndrome virus infection and perspectives on treatments, Viruses 8 (2016) 23.
[33] R. van der Kant, A. Fish, L. Janssen, H. Janssen, S. Krom, N. Ho, T. Brummelkamp, J. Carette, N. Rocha, J. Neefjes, Late endosomal transport and tethering are coupled processes controlled by RILP and the cholesterol sensor ORP1L, J. Cell Sci. 126 (2013) 3462–3474.
[34] R.H. Wijdeven, H. Janssen, L. Nahidiazar, L. Janssen, K. Jalink, I. Berlin, J. Neefjes, Cholesterol and ORP1L-mediated ER contact sites control autophagosome transport and fusion with the endocytic pathway, Nat. Commun. 7 (2016) 11808.
[35] N. Rocha, C. Kuijl, R. van der Kant, L. Janssen, D. Houben, H. Janssen, W. Zwart, J. Neefjes, Cholesterol sensor ORP1L contacts the ER protein VAP to control Rab7-RILP-p150^{Glued} and late endosome positioning, J. Cell Biol. 185 (2009) 1209–1225.